minerals

MDPI

Article

Effect on Fine Particles Output Characteristics of Ceramic Ball Grinding

Jiaqi Tong [1], Caibin Wu [2,*], Yihan Wang [1], Jingkun Tian [1], Zheyang Li [1], Feng Xie [1], Xin Yao [1] and Guisheng Zeng [1]

[1] Jiangxi Key Laboratory of Mining Engineering, Jiangxi University of Science and Technology, Ganzhou 341000, China; 18779320782@163.com (J.T.); wyh3222482679@163.com (Y.W.); tjkjkk@163.com (J.T.); 15579466047@163.com (Z.L.); ad18214990618@163.com (F.X.); yxinyeah@163.com (X.Y.); zengguisheng@hotmail.com (G.Z.)

[2] School of Resources and Environmental Engineering, Jiangxi University of Science and Technology, Ganzhou 341000, China

* Correspondence: caibin.wu@jxust.edu.cn

Abstract: Steel balls as traditional grinding media are prone to excessive fines generation and high energy consumption. Therefore, in light of this problem, the authors investigated another media—ceramic balls based on the output characteristics of fine particles. This study discusses the effect of ceramic balls on the change of the particle size distribution, zero-order output characteristics, micro-strain, and collision energy in ground products. The results showed that for −10 μm particle size, ceramic balls have a smaller production rate than steel balls. In addition, when the filling rate of ceramic balls is 40%, the yield of −10 μm is reduced compared to steel balls. Therefore, ceramic balls greatly reduced the overgeneration of fines. Additionally, the micro-strain rate of ceramic ball grinding with time is 67% lower than that of steel ball grinding. Furthermore, ceramic balls cannot only mitigate excessive fines generation but also effectively reduce energy consumption.

Keywords: ceramic balls; micro-strain; ball mill; excessive fines generation; fines production rate

check for updates

Citation: Tong, J.; Wu, C.; Wang, Y.; Tian, J.; Li, Z.; Xie, F.; Yao, X.; Zeng, G. Effect on Fine Particles Output Characteristics of Ceramic Ball Grinding. *Minerals* **2023**, *13*, 1416. https://doi.org/10.3390/min13111416

Academic Editors: Josep Oliva and Hernán Anticoi

Received: 8 October 2023
Revised: 1 November 2023
Accepted: 2 November 2023
Published: 7 November 2023

1. Introduction

Mineral processing is an important process of mining and comprehensive utilization of mine resources, and grinding is the key process of mineral processing. Over the past few decades, there has been a substantial need for finer grinding in a number of mining projects in order to achieve appropriate liberation, which is necessary for the concentration of important minerals. In comparison to medium-sized particles, both fine and coarse particles have a low flotation recovery. Because fine particles recover at lower rates than coarse fractions, the processing of these particles calls for distinct chemical and hydrodynamic conditions [1]. The low recovery of coarse particles is caused by their strong propensity to detach from bubbles in turbulent settings, whereas that of tiny particles is frequently attributed to the inefficiency of particle–bubble collision [2–4]. In typical flotation conditions, the recovery of small particles is often minimal [5,6]. According to Xu et al. [7], maximum recovery is shown at a size fraction of 38–45 μm. Recovery increases when the size fraction is reduced from 45–75 μm to 38–45 μm. In the whole pH range, recovery then gradually declines when the particle size is further lowered from 38–45 μm to 0–19 μm. Wang et al. [8] noted the three size fractions' constant k values, which are 3.16 for 0.25–0.125 mm, 2.86 for 0.125–0.074 mm, and 2.03 for −0.074 mm. It demonstrated that the medium-size fraction had the highest selectivity, followed by the coarse fraction and the fine fraction. A greater water recovery and worsened entrainment during the flotation process might result from excessive fines generation, which would lower the floatability of ground coking mixtures [9]. However, the energy required for grinding increases with product size, leading to an overall rise in operating expenses that may possibly approach 50% of the cost of mineral processing [10]. Excessive fines generation increases energy

consumption, causes a poor flow of the produced powder, and reduces product yield. Therefore, proper grinding fineness and particle size characteristics are key to successful mineral processing with lower energy consumption.

According to earlier research, the movement of the grinding medium and material consumes 74%–80% of the entire energy, while just 1% was basically utilized to produce new surfaces. The remaining energy inside the mass of impact and friction was transformed into sound and heat energy [11,12]. The traditional grinding media of steel ball has three notable features: First, during the steel ball movement, a capacity density was high [13]. Therefore, in the realization of fine-grained embedded mineral monomer dissociation, it is easy to cause excessive fines generation and affect the subsequent separation recovery. Rather, steel ball grinding will produce iron contamination, affecting the surface flotation characteristics of minerals, which in turn affects the separation index [14]. Third, the steel ball grinding energy consumption is high. As the grinding size becomes increasingly fine, its energy consumption experiences exponential growth. Due to their excellent wear resistance, high hardness, and low-density characteristics, ceramic balls, a revolutionary form of grinding media, can significantly reduce the consumption of grinding power and grinding media when used in stirred mills [15,16]. According to Fang et al. [17], ceramic balls were first used in the secondary mill of the two-stage grinding circuit. The results showed that the grinding products' particle size distribution has clearly improved, leading to a decrease in both the total particle size and the excessive fines generation (10 μm). The distribution of tungsten rose in the −74 μm + 10 μm range and reduced in the 10 μm range as shown in the final product. According to the particle size characteristics of ceramic and steel ball grinding products, ceramic balls have less effect on coarse particles but more impact on grinding fine particles.

The primary goal of this study is to comprehend the features of the ceramic grinding process since there is little research on zero-order production of fines on ceramic ball grinding. It is crucial to study how ceramic ball grinding affects the production of tiny particles in powders. Comparing the experimental findings with the information gained from the well-researched steel ball grinding procedure is a great technique to assess the impact of the ceramic ball grinding process on the characteristics of magnetite powder. This study aims to compare the effects of ceramic and steel balls on the development of fine particle size as well as the effects of the grinding medium on the properties of the powder generated.

2. Theoretical Background

2.1. Zero-Order Output Method

Along with the pace at which the coarser size fractions are ground, another crucial factor in determining how well a mill performs is the rate at which the target size (fine product) is produced. "Zero order production of fines [18,19] is what is meant by this. It is advised that the parameter "zero order output characteristics" be given attention in the grinding circuit since the goal of grinding is to generate tiny particles [20,21]. The zero-order output method assumes that the grinding rate is constant, that is to say, the material shows quite significant zero-order output characteristics at the fine grain level in a short period of grinding time.

$$\frac{dy(x,t)}{dt} = F(x) \tag{1}$$

In the formula, $y(x,t)$ is the cumulative yield of the particle size less than the desired at the moment t; $F(x)$ indicates the zero-order cumulative yield velocity constant for particle size x. Assuming a constant production rate for the fine grain class, $F(x)$ is as follows:

$$F(x) = k\left(\frac{x}{x_0}\right)^{\alpha} \tag{2}$$

α is the particle size distribution index; x_0 is the reference particle size; k is a constant. The simple equation $F(x)$ can also be written as:

$$F(x) = k\left(\frac{x_i}{x_0}\right)^{\alpha} \tag{3}$$

where i = 1, 2, 3 . . . . . ., n (n is the number of different particle sizes generated from the material); $F(x)$ stands for the constant of the fine particle size x_i less than the zero-order output.

2.2. Williamson–Hall and Size-Strain Plot Methods

Due to crystal growth and multi-crystal formation, the crystal size of nanomaterials detected by the area of coherent diffraction differs from the particle size. Crystal flaws cause the strain in the lattice that alters its constant distribution. When these two parameters coexist, the investigated peaks' intensity and breadth increase and the diffraction angle's (2θ) location is altered [22]. A common method for determining the grain size from the width of the diffraction peaks is the Scherrer approach. However, as the peak width is brought on by a combination of lattice strain and particle size, the grain size estimated by this approach is merely an approximation. Williamson–Hall (W-H) analysis, also known as X-ray peak profile analysis, is better suited for estimating the dislocation distribution outside of the TEM picture than the Scherer method since it does not require determining the peak position of the crystal size. Additionally, the W-H approach is a shortened integral breadth way in which peak width as a function of 2θ is used to decouple the strain and size that contribute to peak width. The calculation of crystallite size and strain from XRD data uses the Williamson–Hall (w-h) plot method [23].

Total broadening = broadening due to crystallite size + broadening due to strain

$$\beta_T = \beta_D + \beta_\varepsilon \tag{4}$$

where β_T is the total broadening, β_D is broadening due to crystallite size and β_ε is the broadening due to strain.

We learn from the Scherer equation that

$$D = \frac{K\lambda}{\beta_D COS\theta} \tag{5}$$

Or

$$\beta_D = \frac{K\lambda}{D \cdot cos\theta} \tag{6}$$

where D is the size of the crystallites, θ is the peak location in radians, K = 0.9 is the form factor, λ = 0.15406 nm is the wavelength of the X-ray source, and β_D is the FWHM (i.e., broadening of the peak) in radians.

Similar to this, the XRD peak widening caused by microstrain is provided by

$$\beta_\varepsilon = 4\varepsilon tan\theta \tag{7}$$

where β_ε is the strain-induced widening, ε is the strain, and θ is the radian location of the peak. Equation (1) is formed by combining Equations (6) and (7):

$$\beta_T = \frac{K\lambda}{D \cdot cos\theta} + 4\varepsilon tan\theta \tag{8}$$

As we know, $tan\theta = sin\theta / cos\theta$. Therefore, Equation (8) is represented by

$$\beta_T = \frac{K\lambda}{D \cdot cos\theta} + \frac{4\varepsilon sin\theta}{cos\theta}$$

Multiplying both sides by $cos\theta$,

$$\beta_T \cdot cos\theta = \frac{K\lambda}{D} + 4\varepsilon sin\theta$$

Or

$$\beta_T cos\theta = \varepsilon(4sin\theta) + \frac{K\lambda}{D} \quad (9)$$

Equation (9) depicts a straight line, with $K\lambda/D$ serving as the y-intercept and as the gradient (slope) of the line.

3. Experimental

3.1. Material and Grinding Media

Particle size particles in the grinding process differ with crushing rate [8]. In order to better reflect the grinding effect of ceramic balls in fine grinding, a magnetite ore sample was split into different size classes with a vibrating screening classifier. Table 1 presents the granulometric composition of the initial samples. The following single-sized feeds were created: 0.3 + 0.212 mm, 0.212 + 0.15 mm, 0.15 + 0.106 mm, 0.106 + 0.075 mm, and 0.075 + 0.038 mm. For the following reasons, grinding balls were chosen in the manner shown in Table 2: In tiny laboratory mills (20 cm in diameter or less), it was first observed that only balls smaller than 40 mm may demonstrate substantial media effects on grinding kinetics [23]. Second, it was found that the ratio of the mill cylinder's diameter to the largest ball size should be at least 6:1. For instance, in Bond's ball mill work index test, the ratio was 8:1 [24], and in Lee's (2019) grinding kinetic test, 25.4 mm balls were chosen to match a U_{20} cm mill with 1–2 cm lifters [25]. Furthermore, it is assumed that because the Φ15 mm steel balls and φ15 ceramic balls used in this study shared the same centrifuge, their charge motion and impact frequency are the same.

Table 1. The granulometric composition of the initial samples.

Size/mm	Mass Yield/%	Cumulative Passing/%
1.18	2.16	100.00
0.5	8.38	97.84
0.3	41.34	89.46
0.15	33.89	48.13
0.075	6.45	14.23
0.038	2.73	7.78
0.0.23	4.47	5.05
0.019	0.34	0.59
0.010	0.25	0.25
sum	100	-

Table 2. The characteristics of the two types of balls.

Type	Bulk Density (g/cm^3)	Physical Density (g/cm^3)	Elements	Trace Element	Mohs Hardness	Filling Rate (%)
Ceramic ball	2.22	3.7	Al, Si	Ca, Mg	6.8	40
Steel ball	4.85	7.3~7.8	Fe, Cr, C	Si, Mn, P, Mo	9	40

3.2. Experimental Procedures

The grinding experiments were performed in a batch mill with 150 mm in height and 130 mm in diameter, with a capacity of 2000 cm^3, and four lifters inside. The predetermined speed is 170 rev/min, the mill speed is 98 rpm (118 rpm). For each test, 200 g of single-sized class sample and 100 mL of tap water were required to create a mill charge with a 67% solids concentration. Figure 1 depicts an illustration of the grinding apparatus between the rollers. To calculate the cumulative mass distribution of the product, the samples were sieved using

a set of conventional laboratory sieves with the following mesh sizes: 300 μm, 212 μm, 150 μm, 106 μm, 75 μm, 38 μm, and 23 μm. The laser particle size measurement equipment was used to determine the relative mass distributions of the ground products. The effects of grinding on the properties of the ground products were then analyzed using XRD, involving changes in micro-strain and grain size as well as mineral surface morphology. First, the grinding effects of the two media were compared, including the particle size distribution and zero-order output characteristics of the ground products. Finally, this phenomenon was explained using the ball mill motion hypothesis.

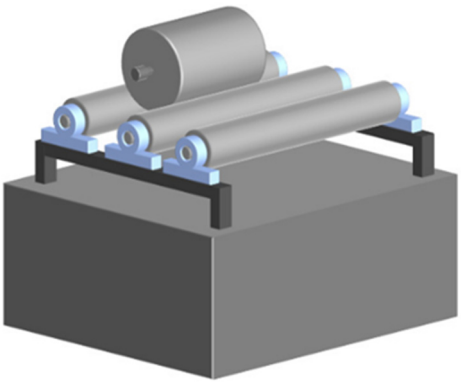

Figure 1. Schematic of the grinding equipment used in the grinding process [26].

4. Results and Discussion

4.1. Cumulative Size Distributions

The cumulative particle size curves for the steel ball and ceramic ball at various grinding periods are shown in Figure 2. In comparison to the ceramic ball, the steel ball showed a quicker reduction in average particle size (d_{50}) as the grinding period increased from 2 min to 10 min. This is brought on by the various grinding media conditions' varying breakage energies and grinding environments. It has been shown that particle fracture is a random process and that increasing impact energy may effectively increase fracture probability [27]. Moreover, the specific gravity of steel balls is much higher than that of ceramic balls, and the force of a single collision of steel balls is much greater than that of ceramic balls [28].

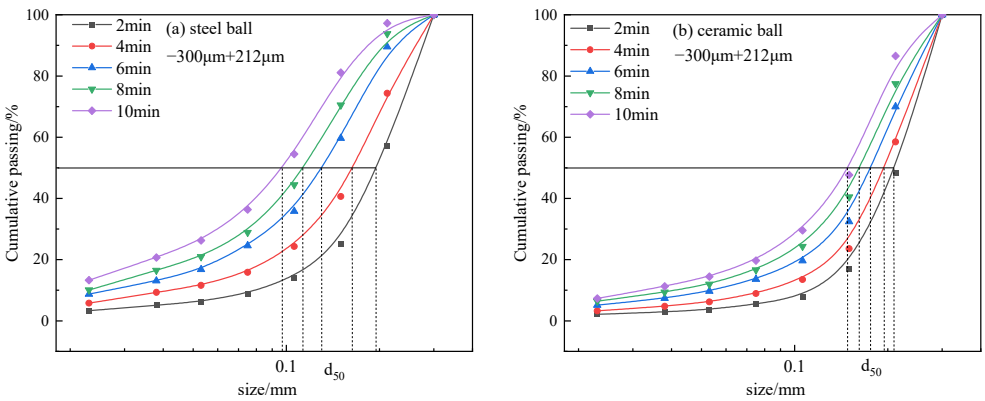

Figure 2. *Cont.*

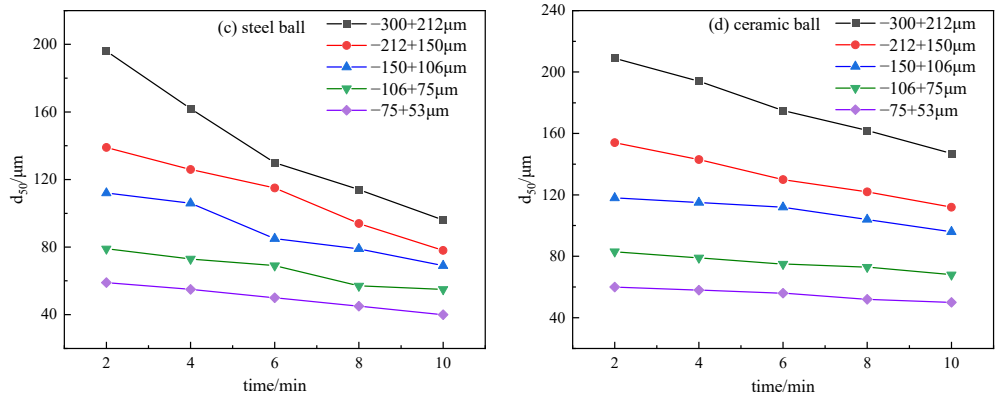

Figure 2. Size distribution of (**a**) steel and (**b**) ceramic ball grinding products with grinding time; d_{50} of (**c**) steel and (**d**) ceramic ball grinding products with grinding time.

Due to the significant increase in contact energy between the balls and small particles, the production rates for steel ball grinding and ceramic ball grinding rose to 53 μm, 38 μm, 23 μm, and 10 μm, respectively (see Figures 3 and 4). It should be noted that steel ball grinding yields more output of 53 μm, 38 μm, 23 μm, and 10 μm than ceramic ball grinding in a short period of time. In general, steel ball grinding is more efficient than ceramic ball grinding in reducing the particle size of a wide range of materials to submicron scale. The quantity of excessive fines generation for steel ball grinding thus becomes larger as the grinding duration rises than it does for ceramic ball grinding.

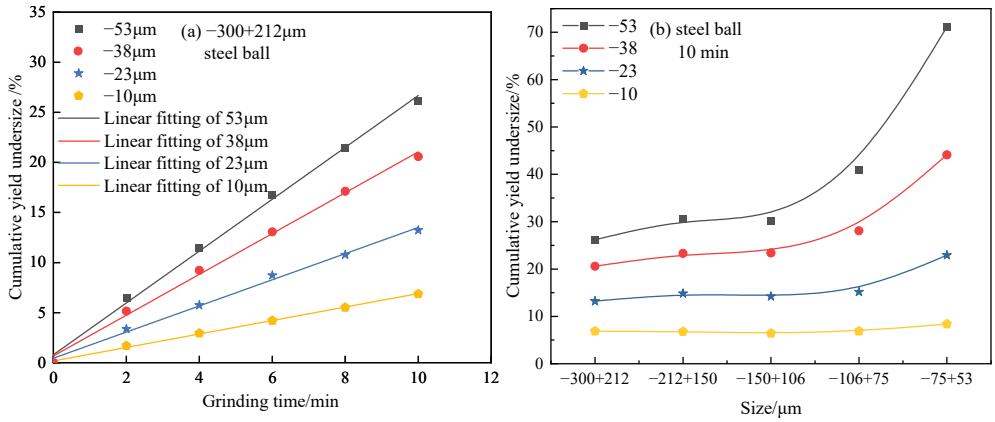

Figure 3. (**a**) Cumulative distribution function of steel ball grinding with the same total weight; (**b**) the % fines produced of steel ball at the end of 10 min.

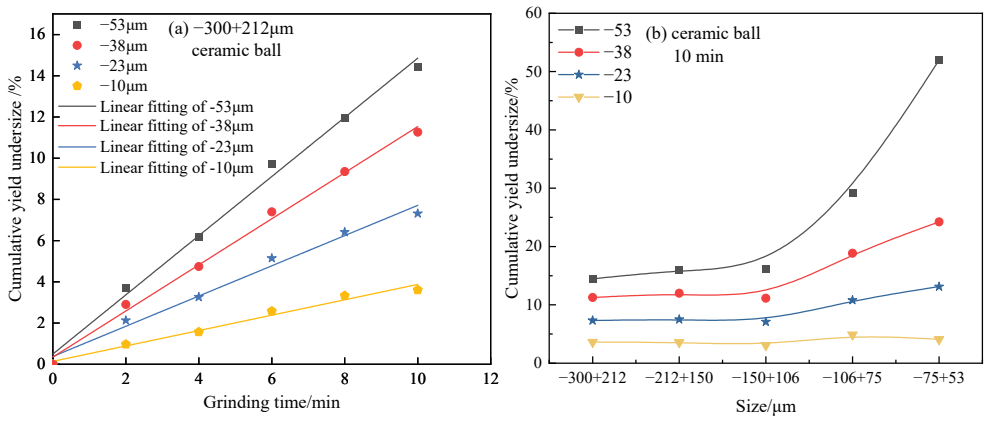

Figure 4. (**a**) Cumulative distribution function of ceramic ball grinding with the same total weight; (**b**) the % fines produced of ceramic ball at the end of 10 min.

In mineral separation, the lower limit of particle size differs with different feeds, and as the common lower limit is at (−10 + 0) μm, they are selected as examples in this study. Figure 5 shows the relationship between $F_{10\mu m}$ and the feed particle sizes. In the case of different feed sizes, the production rate of (−10 + 0) μm grade of steel ball grinding is greater than that of ceramic ball grinding. That is, the steel ball will produce more ultra-fine particles. It can be seen in Figure 5 shows that the $F_{10\mu m}$ of the steel ball as grinding media remains stable with the decrease in grinding grain size, with an average value of 0.65, while the $F_{10\mu m}$ of the ceramic ball as grinding media remains stable, with an average value of 0.35. This indicates that the production rate of (−10 + 0) μm does not change with the particle size in the grinding process of either ceramic ball or steel ball, but the $F_{10\mu m}$ of steel ball is twice as high as that of ceramic ball. This shows that steel balls are more energy consuming in producing ultra-fine particle size (relatively ultra-fine particle size fraction). That is, the material is subjected to greater stress when the steel ball is used as the grinding media.

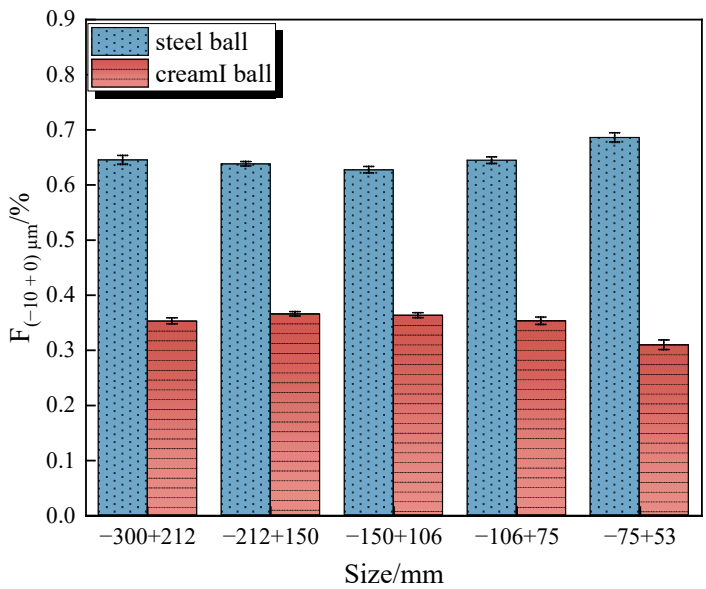

Figure 5. (−10 + 0) μm fine produced by single-sized class samples with steel balls and ceramic balls.

Figure 6 shows a linear regression on the constant α derived from the exponential function. From the figure, it can be seen that the relationship between F_i and x_i approximates $F_i = kx_i^{\alpha}$, where k and α are constants. Constant values of α are obtained by fitting different particle sizes, which are shown in Table 3. The values of α acquired by steel ball grinding and ceramic ball grinding of the same particle size are basically the same, where α solely pertains to the material's inherent crushing properties and has nothing to do with mill size or grinding conditions. The values obtained with steel and ceramic balls as grinding media in this study are not exactly the same. This is mainly due to the experimental error factor. However, as the particle size decreases, the value of α increases. This is because different crystal interfaces and surface cracks at different particle sizes result in different degrees of difficulty in crushing.

Table 3. The constant α derived from the exponential function.

Type \ Size/μm	−300 + 212	−212 + 150	−150 + 106	−106 + 75	−75 + 53
Steel ball	0.94	1.07	1.14	1.17	1.27
Ceramic ball	0.93	1.06	1.13	1.18	1.27

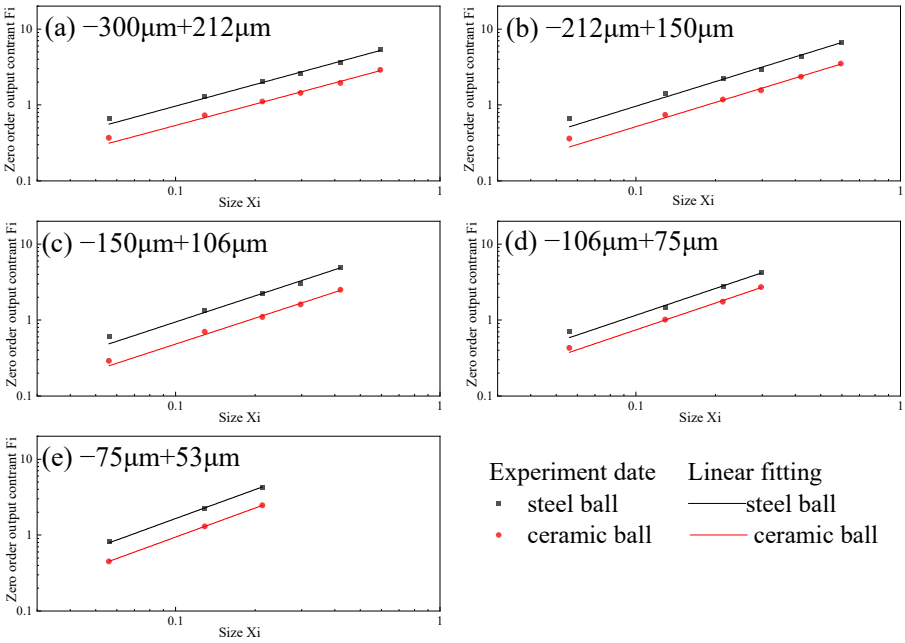

Figure 6. Comparison of zero-order output constants.

4.2. Properties Analysis of Micro-Strain

Figure 7 displays the X-ray diffraction patterns of the ball-milled magnetite powders produced with various grinding media. Table 4 shows the average values for the locations of the magnetite peaks in Figure 7. As can be seen, peak position increases with grinding time and more peaks shift with ceramic balls, which is caused by an increase in grinding energy. The position of the peaks of steel ball grinding is clearly higher than that of ceramic balls because steel balls consume more milling energy than ceramic balls. Figure 7 also shows the magnetite phase in the magnetite powder emergence of anhydrite when grinding with ceramic and steel balls. Since finer particles usually have higher surface energies and are more reactive with carbon in the environment, they react with the carbon in the cemented carbide milling balls as the milling energy increases.

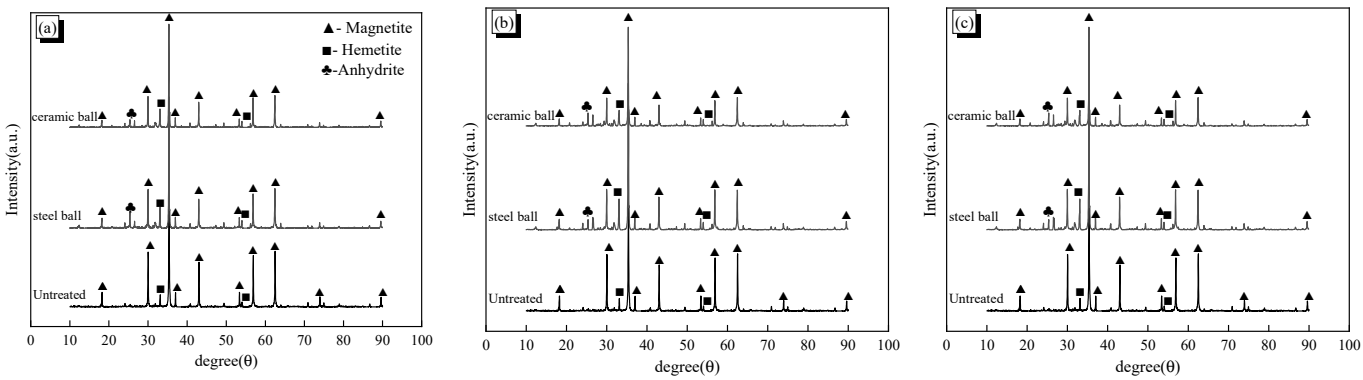

Figure 7. XRD patterns of different magnetite powders ((**a**) 2 min, (**b**) 6 min, (**c**) 10 min).

Table 4. The change of average peak position in radians over time.

θ	0 min	2 min	4 min	6 min	8 min	10 min
steel	0.358	0.352	0.349	0.348	0.347	0.344
ceramic	0.358	0.344	0.326	0.325	0.324	0.322

Figure 8, which presents the findings of the Williamson–Hall analysis of the XRD data [22], illustrates the average crystallite size and strain of magnetite powder. These

data demonstrate that the strain somewhat decreases during ceramic ball grinding while the crystallite size remains constant. The information in Figure 8 further reveals that the crystallite size of the untreated magnetite powder is 47.24 nm and that the lattice strain is about 3.63. After being ground in a ceramic ball mill, this powder's lattice strain rises to 6.31, while the crystallite size remains within the 40–46 nm range. Following ceramic ball grinding, the powder's lattice strain rises while the size of the crystallites remains almost the same.

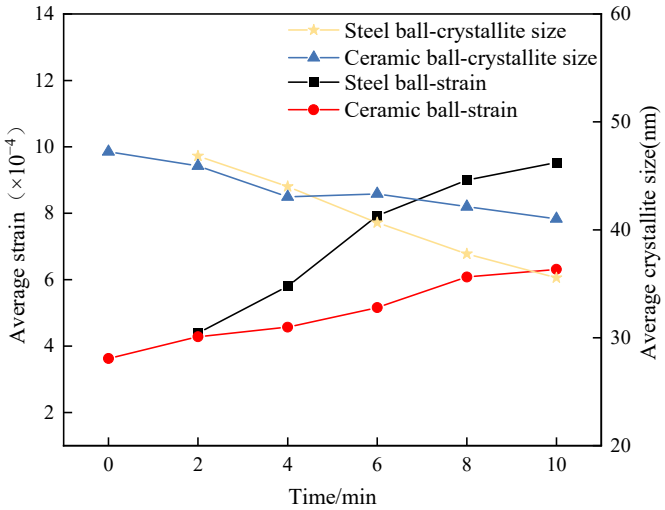

Figure 8. Relationship between average crystallite size/strain of magnetite powder and steel ball grinding/ceramic ball grinding time.

During the ball milling procedure, the particles are subjected to high-energy impacts, which cause plastic deformation and breakage. A smaller crystallite and increased lattice strain are caused by the formation of correlated arrangements of the defects, such as dislocation walls or small-angle grain borders (sub-grain). The line broadening of X-ray peaks, which is clearly seen in Figure 8, indicates the existence of a high density of microstructure defects in magnetite powder. This indicates that ceramic ball grinding has a unique impact on fine and ultrafine powders without generating more ultrafine particle size in a short period of time. This outcome is comparable to the examination of the finished product's particle size distribution. The lattice strain of steel ball grinding is greater than that of the ceramic ball, and the powder crystallite size of the steel ball grinding is smaller than that of the ceramic ball. According to prior studies, steel medium is easier to work with to create products that are somewhat less oversized than ceramic balls of the same mass and surface area [29]. However, in mineral separation, the finer particle sizes are not always the better. Excessive fines generation can be detrimental to the separation and the beneficiation index. The low density and high hardness of ceramic balls effectively reduce the generation of excessive fine generation particles in the grinding process compared to steel balls.

Figures 8 and 9 also show that for 10 min grinding with steel balls and ceramic balls, the strain increases quickly from 3.63 to 9.53 and from 3.63 to 6.31, respectively. The slope of the linear fit is 0.67 and 0.22, respectively. The speed of the growth of lattice strain is significantly higher in steel balls than in ceramic balls. The strain increases with the decrease of θ (Figure 7 and Table 4) and crystallite size decreases with the decrease of θ. The difference in the strain between the ceramic and steel ball products increases after four minutes of grinding. The difference in crystallite size between the ceramic and steel ball products increases after 2 min of grinding. This indicates that steel balls use higher energy to act on the powder in the grinding process compared to ceramic balls, so it is safe to say that steel balls consume more energy than ceramic balls.

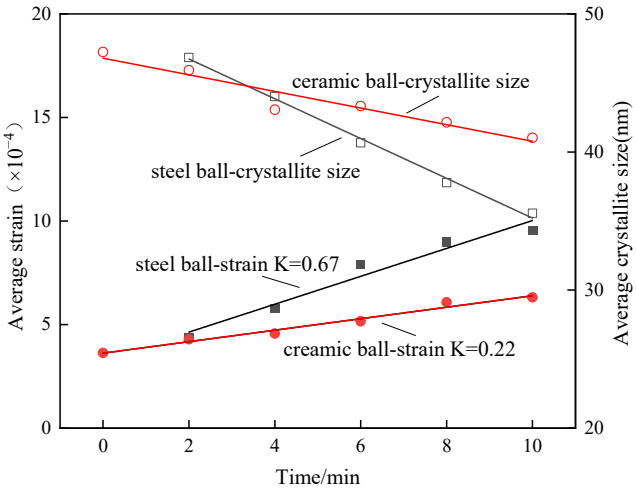

Figure 9. Linear fitting between average crystallite size/strain of magnetite powder and steel ball grinding/ceramic ball grinding time.

4.3. Energy Influence by Mill Media

Figure 10 represents the throw-down operating state of the ball mill. On a circular trajectory AB of radius *R*, the length L of the speech mill divides an infinitely thin media layer of thickness dR from the total ball charge. In the time interval of one week of cylinder rotation, the weight of this media layer is:

$$dG = 2\pi RL\delta dR \text{ (t)}$$

$$dG = 2000\pi RL\delta dR \text{ (kg)}$$

where *L* is the ball mill frontal length, m; *R* is the distance from the center of the circle of the media at the location, m; δ is the density of the ball pile, t/m^3.

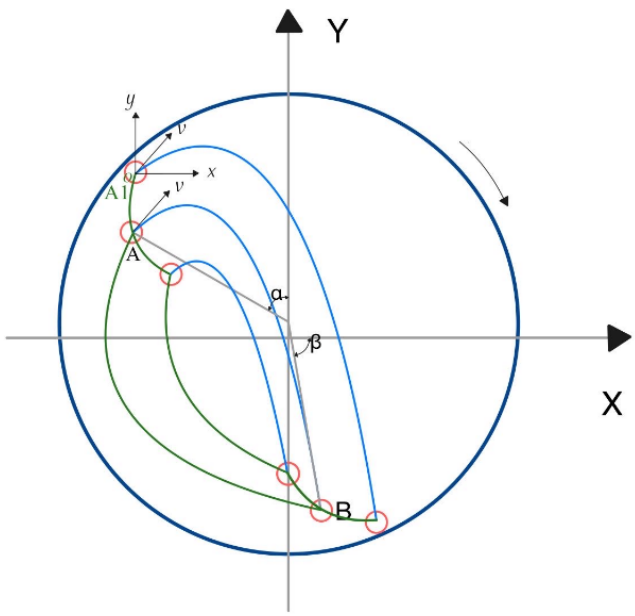

Figure 10. The cataracting trajectory of grinding media.

The mass of the media is:

$$dm = \frac{dG}{g} = \frac{2000\pi L\delta dR}{g}$$

The kinetic energy of the grinding media falling to a circular trajectory is:

$$E = \frac{mv^2}{2}(9 - 8cos^2\alpha)$$

Ceramic balls have a lower specific gravity and better wear resistance than conventional media of steel balls [30]. Because they could be employed to achieve quick stirring rates while preserving high kinetic energy and having low specific gravity, ceramic balls were first used exclusively in the Isa Mill [31]. The kinetic energy of ceramic balls and steel balls doing throwing down motion in the mill is E_1 and E_2, respectively. Since the bulk density of ceramic balls is 2.22 and that of steel balls is 4.75, $E_2 \approx 2E_1$. The energy of the ceramic ball applied to the mineral is smaller than that of the steel ball, so the micro-strain produced by the ceramic ball on the mineral is smaller than that of the steel ball, which is consistent with the description of the change of micro-strain above. Figure 11a,b shows the surface morphology of the steel ball grinding product particles, the surface is relatively rough; Figure 11c,d represents that the ceramic ball grinding product particles' surface morphology is relatively flat and smooth. Steel balls have higher density, high energy consumption during grinding, and high instantaneous collision force between ball and ball, ball and ore, and ball and mill. High kinetic energy is generated during grinding, much greater than the kinetic energy required to crush the ore to qualified particle size. This results in high energy loss, and thus it is easier to cause excessive fines generation than ceramic balls. This is in agreement with the above description, steel ball grinding produces a much higher yield of overfine particles than ceramic balls.

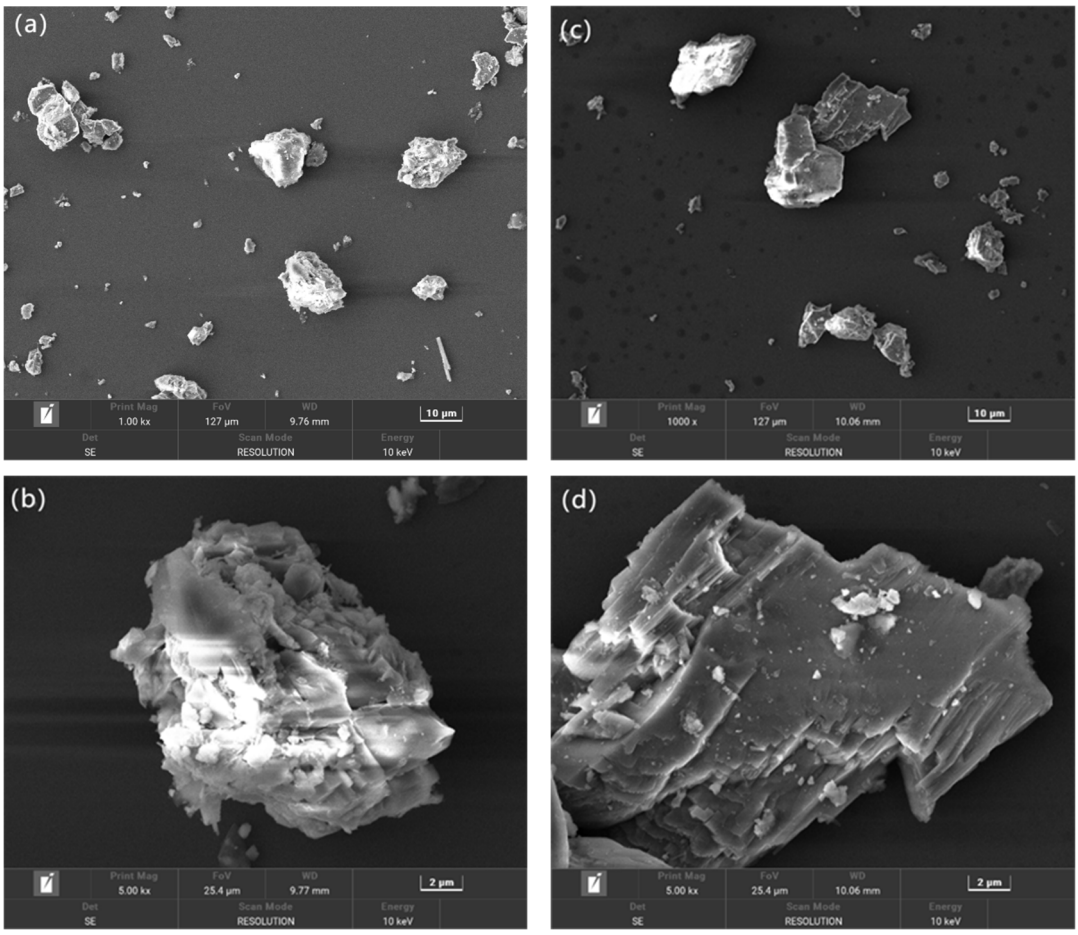

Figure 11. The morphology of the ground particles with SEM micrographs: (**a**,**b**) steel ball; (**c**,**d**) ceramic ball.

5. Conclusions

Ceramic ball grinding can reduce excessive fines generation. Excessive fines generation affects the particle size characteristics of the grinding product, degrades the product quality, and increases the energy expense. The study demonstrates that less excessive fine generation can be achieved with ceramic ball mills. The main findings of the paper are as follows:

(a) The zero-order output characteristic constant α increases with the decrease in the particle size. With the same feeding size, steel balls and ceramic balls have the same value of α. Steel balls as grinding media have a higher Fx in the grinding process than ceramic balls. And in a short time, the yield of ceramic balls ((−10 + 0) μm) is reduced compared to steel balls, and ceramic balls as fine grinding media can reduce excessive fines generation.

(b) The results of the XRD analysis show that the micro-strain rate of ceramic ball grinding with the change of time is 67% lower than that of steel ball, and the grain size of both ceramic and steel ball grinding products decreases slightly, but the product size of steel balls is smaller than that of ceramic balls.

(c) The specific gravity of ceramic balls is small, and the instantaneous collision kinetic energy is small in the grinding process. Grinding with ceramic balls produces a smaller amount of excessive fine-generation particle size for fine-grained grinding ore.

Author Contributions: Conceptualization, J.T. (Jiaqi Tong) and C.W.; methodology, J.T. (Jingkun Tian); validation, Y.W., Z.L. and F.X.; formal analysis, X.Y.; investigation, J.T. (Jiaqi Tong); data curation, C.W.; writing—original draft preparation, J.T. (Jiaqi Tong); writing—review and editing, C.W.; resources, J.T. (Jingkun Tian); supervision, funding acquisition, C.W. and G.Z. All authors have read and agreed to the published version of the manuscript.

Funding: This work was financially supported by the National Key Research and Development Program of China: 2022YFC2905103-01.

Data Availability Statement: For certain policy reasons, it is not convenient to publicize the data in this paper. However, if interested in the research of this paper, you can email us for the data.

Acknowledgments: The authors would also like to thank the Jiangxi Key Laboratory of Mining Engineering and Hunan Shizhuyuan Nonferrous Metals Co., Ltd., China, for their support. Yuqing Wang from the Jiangxi University of Science and Technology is also gratefully acknowledged.

Conflicts of Interest: The authors declare no conflict of interest.

References

1. Pease, J.D.; Curry, D.C.; Young, M.F. Designing flotation circuits for high fines recovery. *Miner. Eng.* **2006**, *19*, 831–840. [CrossRef]
2. Fuerstenau, D.W.; Abouzeid, A.Z.M. The energy efficiency of ball milling in comminution. *Int. J. Miner. Process.* **2002**, *67*, 161–185. [CrossRef]
3. Gontijio, C.D.; Fornasiero, D.; Ralston, J. The Limits of fine and coarse particle flotation. *Can. J. Chem. Eng.* **2007**, *85*, 739–747. [CrossRef]
4. Farrokhpay, S.; Filippov, L. Aggregation of nickel laterite ore particles using polyacrylamide homo and copolymers with different charge densities. *Powder Technol.* **2017**, *318*, 206–213. [CrossRef]
5. Sivamohan, R. The problem of recovery of very fine particles in mineral processing—A review. *Int. J. Min. Process.* **1990**, *28*, 247–288. [CrossRef]
6. Rulyov, N.N. Turbulent microflotation: Theory and experiment. *Colloid. Surf. A* **2001**, *192*, 73–91. [CrossRef]
7. Xu, L.; Hu, Y.; Wu, H.; Tian, J.; Liu, J.; Gao, Z.; Wang, L. Surface crystal chemistry of spodumene with different size fractions and implications for flotation. *Sep. Purif. Technol.* **2016**, *169*, 33–42. [CrossRef]
8. Wang, Y.; Mu, H.; Li, X.; Yuan, J.; Chen, J.; Xiao, S.; Bao, Q.; Gao, Y.; He, J. Observation of large nonlinear responses in a graphene-Bi2Te3 heterostructure at a telecommunication wavelength. *Appl. Phys. Lett.* **2016**, *108*, 221901. [CrossRef]
9. Prziwara, P.; Kwade, A. Grinding aids for dry fine grinding processes—Part I: Mechanism of action and lab-scale grinding. *Powder Technol.* **2020**, *375*, 146–160. [CrossRef]
10. Vieira, M.G.; Peres, A.E.C. Effect of rheology and dispersion degree on the regrinding of an iron ore concentrate. *J. Mater. Res. Technol.* **2013**, *2*, 332–339. [CrossRef]

11. Levesque, M.Y.; Millar, D.L. The link between operational practices and specific energy consumption in metal ore milling plants—Ontario experiences. *Miner. Eng.* **2015**, *71*, 146–157. [CrossRef]
12. Radziszewski, P. Assessing the stirred mill design space. *Miner. Eng.* **2013**, *419*, 16. [CrossRef]
13. Burger, R.; Menendez-Aguado, J.M.; Fulla, M.R.; Rivera, I.E. Study of steel ball recharge and consumption in a wet cement industrial mill via a population balance model. *Particul. Sci. Technol.* **2022**, *40*, 972–979. [CrossRef]
14. Cheng, G.; Liu, J.T.; Gui, X.H.; Hu, Z.B.; Wang, Y.T. Effect of different grinding conditions on the dissociation and flotation of difficult-to-float coal. *Energ. Source Part A* **2016**, *38*, 1103–1109. [CrossRef]
15. Hassall, P.; Nonnet, E.; Keikkala, V.; Komminaho, T.; Kotila, L. Ceramic bead behavior in ultra fine grinding mills. *Miner. Eng.* **2016**, *98*, 232–239. [CrossRef]
16. Zhang, X.; Qin, Y.; Han, Y.; Li, Y.; Gao, P.; Li, G.; Wang, S. A potential ceramic ball grinding medium for optimizing flotation separation of chalcopyrite and pyrite. *Powder Technol.* **2021**, *392*, 167–178. [CrossRef]
17. Fang, X.; Wu, C.; Liao, N.; Yuan, C.; Tong, J. The first attempt of applying ceramic balls in industrial tumbling mill: A case study. *Miner. Eng.* **2022**, *180*, 107504. [CrossRef]
18. Herbst, J.A.; Fuerstenau, D.W. The zero-order production of fine sizes in comminution and its implications in simulation. *Trans. AIME* **1968**, *241*, 538–546.
19. Gupta, V.K. Zero order production of fines in ball and rod mill grinding: An explanation. In Proceedings of the SME-AIME Annual Meeting, New York, NY, USA, 24–28 February 1985; pp. 85–139.
20. Gupta, V.K. The Estimation of Bate and Breakage Distribution P ammeters from Batch Grinding Data for a Complex Pyritic Ore Using a Back-Calculation Method. *Powder Technol.* **1981**, *28*, 97–106. [CrossRef]
21. Venkataraman, K.S. Application of the Population Balance Model to the Grinding of Mixtures of Minerals. *Powder Technol.* **1984**, *39*, 133–142. [CrossRef]
22. Zak, A.K.; Majid, W.H.A.; Abrishami, M.E.; Yousefi, R. X-ray analysis of ZnO nanoparticles by Williamson–Hall and size–strain plot methods. *Solid State Sci.* **2011**, *13*, 251–256.
23. Mclvor, R.E. The effect of media sizing on ball grinding efficiency. In *Comminution Practices, Society for Mining*; Kawatra, S.K., Ed.; Metallurgy and Exploration, Inc.: Littleton, CO, USA, 1997; pp. 279–292.
24. Bond, F.C.; Maxson, W.L. Standard grindability tests and calculations. *Trans. SME-AIME* **1943**, *153*, 362–372.
25. Lee, H.; Kim, K.; Lee, H. Analysis of grinding kinetics in a laboratory ball mill using population-balance-model and discrete-element-method. *Adv. Powder Technol.* **2019**, *30*, 2517–2526. [CrossRef]
26. Liao, N.; Wu, C.; Li, J.; Fang, X.; Li, Y.; Zhang, Z.; Yin, W. A Comparison of the Fine-Grinding Performance between Cylpebs and Ceramic Balls in the Wet Tumbling Mill. *Minerals* **2022**, *812*, 1007. [CrossRef]
27. Deniz, V. Relationships between Bond's grindability (G(bg)) and breakage parameters of grinding kinetic on limestone. *Powder Technol.* **2004**, *139*, 208–213. [CrossRef]
28. Austin, L.G.; Shah, J.; Wang, J.; Gallagher, E.; Luckie, P.T. An analysis of ball-and-race milling: Part I. The Hardgrove mill. *Powder Technol.* **1981**, *29*, 263–275. [CrossRef]
29. Shi, F. Comparison of grinding media-Cylpebs versus balls. *Miner. Eng.* **2004**, *17*, 1259–1268. [CrossRef]
30. Yu, J.; Qin, Y.; Gao, P.; Han, Y.; Li, Y. An innovative approach for determining the grinding media system of ball mill based on grinding kinetics and linear superposition principle. *Powder Technol.* **2021**, *378*, 172–181. [CrossRef]
31. Curry, J.A.; Ismay, M.J.; Jameson, G.J. Mine operating costs and the potential impacts of energy and grinding. *Miner. Eng.* **2014**, *56*, 70–80. [CrossRef]